Superconductivity in Zr_5Al_4 intermetallic compound

Zuzanna Sobczak[1,*], M.J. Winiarski[1], W. Xie[2], R. J. Cava[3], T. Klimczuk[1,†]

[1]*Faculty of Applied Physics and Mathematics, Gdansk University of Technology, Narutowicza 11/12, 80-233 Gdansk, Poland*

[2]*Department of Chemistry, Louisiana State University, Baton Rouge, LA, USA 70803*

[3]*Department of Chemistry, Princeton University, Princeton New Jersey 08544, USA*

* zuzanna.sobczak@pg.edu.pl

† tomasz.klimczuk@pg.edu.pl

Polycrystalline compound Zr_5Al_4 was synthesized using the arc-melting method. Powder x-ray diffraction confirms previously reported crystal structure of Ti_5Ga_4-type (*P6₃/mcm*) with lattice parameters: a = 8.4312(6) Å, and c = 5.7752(8) Å. The electrical resistivity and low temperature magnetic susceptibility studies indicate that Zr_5Al_4 exhibits superconducting behavior. The normalized heat capacity jump at T_c = 1.82 K is $\Delta C/\gamma T_c$ = 1.41 and confirms bulk superconductivity. The Sommerfeld coefficient γ = 29.4 mJ mol^{-1} K^{-2} and the Debye temperature Θ_D = 367 K were obtained by fitting the low temperature heat capacity data. The electron-phonon coupling strength $\lambda_{el\text{-}ph}$ = 0.48 and estimated upper critical field $\mu_0 H_{c2}(0)$ = 1.09 T (dirty limit) suggest that Zr_5Al_4 is a weakly coupling type-II superconductor. The first-principles calculations show presence of the van Hove singularity near the Fermi that plays the significant role in the superconductivity.

I Introduction

Superconductivity has been an interesting topic for scientific community since its discovery in 1911 in mercury. Prediction of a new superconducting materials remains challenging task and several approaches were invented until now. Finding superconductivity in structural families gives the odds of discovering new superconductors. One of the ideas is to look for endohedral gallide cluster building blocks [1] and there are already several members of this superconducting system [1–6]. Due to the similarity to gallium, aluminum is a good candidate

to further expand this search. For example, superconductivity was found in MT_2Al_{20} (M=Sc, Lu, Y, La, Pr; T = Ti, V, Nb, Ta) cage compounds [7–10] and is likely driven by a rattling effect postulated in ref. [7–10].

Endohedral cluster compounds are usually built of alkali or alkaline-earth metals that donate electrons to stabilize the structure. The less obvious candidate that could also create such cluster is Zr. Its electronegativity (χ = 1.33 in Pauling's scale [11]) places Zr in the vicinity of atoms that are usually referred to as stabilizing the structure such as Mg (χ = 1.31) or Na (χ = 0.93). Therefore, Zr in Zr-Al bond is a weak electropositive donor of electrons (χ(Zr) = 1.33, χ(Al) = 1.61), thus from the chemical point of view fulfills the requirements for forming an endohedral cluster.

Zr_5Al_4 was first reported as an additional phase in Zr_3Al_2 sample [12]. It is a member of Ti_5Ga_4-type family, with a crystal structure consisting of Al decahedra surrounding one site of Zr atoms, as shown in Fig. 1. $ZrAl_7$ cluster can be considered as a building block of the structure, similarly to Zr_2Al_3 where the cluster consists of 8 Al atoms [13,14]. Since obtaining pure Zr_5Al_4 is nontrivial, the physical properties were unknown until now. Density functional theory (DFT) calculations of the electronic structure shows that the van Hove singularity around the Fermi level is important for the superconductivity in Zr_5Al_4. Metastable character of Zr_5Al_4 is reflected in the results of high throughput DFT calculations on Zr-Al systems, as the calculated total energy places the phase above the convex hull [15,16].

Here we describe for the first time synthesis and physical properties of a type-II superconductor Zr_5Al_4 by means of magnetization, heat capacity and electrical resistivity.

II Materials and Methods

A polycrystalline sample of Zr_5Al_4 was synthesized by arc-melting elemental zirconium (rod, 99.2%, Alfa Aesar) and aluminum (shot, 99.99%, Alfa Aesar) in the MAM-1 Edmund Buhler arc furnace on a water cooled copper hearth with high purity argon (5N) atmosphere. After each melting a sample button was turned and re-melted several times to ensure homogeneity. Estimated mass loss was around 1% and was compensated by 2% excess of Al. The as-cast sample was used for the structural and physical studies.

The phase purity of a crushed sample at room temperature was evaluated using powder x-ray diffraction (PXRD) on the Bruker D2 Phaser 2nd generation diffractometer using Cu-Kα

radiation and a LynxEye XE-T detector. PXRD pattern was analyzed using Pawley fit [17] with the Diffrac.SuiteTopas software [18].

All measurements were performed using a Quantum Design Dynacool Physical Property Measurement System (PPMS). For magnetic susceptibility studies a vibrating sample magnetometer (VSM) technique was employed. Heat capacity was done on a polished sample using the standard 2τ relaxation method in in the system equipped with ^{3}He cooling. Electrical resistivity was conducted on a sample with Pt (50 μm dia.) wires that were spark welded to a polished flat sample surface.

The band structures and Density of States (DOS) of Zr_5Al_4 were calculated using the Wien2K with local density approximation (LDA)-type pseudopotentials. The electronic structure with and without the spin-orbit coupling (SOC) were performed on all atoms. Reciprocal space integrations were completed over an 6×6×8 Monkhorst-Pack *k*-points mesh. The convergence criterion for self-consistent field calculation is 0.1meV.

III Results

The room temperature PXRD measurement was performed in order to confirm phase purity of Zr_5Al_4 sample. The result is presented in Fig. 2. All the Bragg lines in the PXRD pattern are indexed with a hexagonal *P6$_3$/mcm* unit cell of Ti_5Ga_4 type. Pawley fit represented by a black solid line in Fig. 2 gave the lattice parameters: a = 8.4312(6) Å and c = 5.7752(8) Å, which are in good agreement with values reported previously [12]. Details of the Pawley analysis of the diffraction pattern in comparison with lattice parameters from ref. [12] are presented in Table 1. The sample is stable in air, and does not show any signs of decomposition after 14 days. The as-cast sample was found to be of the highest purity. All the annealing experiments performed at temperatures between 1000^{o}C and 1150^{o}C and for 12 hours up to 2 days, revealed presence of impurity phases, or complete decomposition of Zr_5Al_4. That is in agreement with a proposed Zr – Al phase diagram [15], which shows that Zr_5Al_4 is a high temperature phase. Air or water quenching after the annealing did not result in obtaining a single Zr_5Al_4 compound.

The observed instability of Zr_5Al_4 is in agreement with the results of DFT total energy calculations available in the Materials Project database [19]. Zr_5Al_4 is 45 meV above the convex hull for the Zr-Al system [16] and is neighbored by two stable phases: Zr_4Al_3 and Zr_2Al_3 [20,21] to which it decomposes upon annealing.

To characterize the superconducting transition of Zr_5Al_4, zero-field cooled (ZFC) and field cooled (FC) dc volume susceptibility $\chi_V = M_V/H$ was measured in the temperature range of 1.68 – 2.4 K, with a small magnetic field H = 10 Oe. The results are shown in a main panel of Fig. 3. The superconducting transition temperature T_c = 1.94 K is defined as the temperature where the extrapolation of the steepest slope of χ(T) intersects the extrapolation of the normal state susceptibility to lower temperatures [22]. At the lowest temperature χ_V starts to saturate and the magnetic susceptibility $4\pi\chi_V$ is -1.2. A stronger than expected ($4\pi\chi_V$ = -1) diamagnetic signal is due to a fact that we do not consider a demagnetization effect. The inset of Fig 3. presents magnetization vs. magnetic field M(H) collected at 1.7 K. The shape of M(H) curve suggests that Zr_5Al_4 is a type-II superconductor and a lower critical field at T=1.7 K is equal to μ_0H_{c1}(1.7K) = 16 Oe. Magnetic measurements below 1.68 K are required for more detailed analysis in order to estimate the demagnetization factor (N) and the lower critical field $H_{c1}(0)$.

The temperature dependence of heat capacity C_p(T) measured in the presence of superconducting transition is presented in Fig. 4 a). The bulk nature of the superconductivity in Zr_5Al_4 is confirmed by a sharp anomaly seen at temperature T_c = 1.82 K, which is slightly lower than T_c obtained from the magnetic susceptibility measurement. The value of a specific heat jump at T_c, estimated with the equal entropy construction method, is $\Delta C/T_c$ = 42.8 mJ mol^{-1} K^{-2}. Fig. 4 c) shows a plot of C_p/T versus T^2, measured in an applied field of 0.2 T. A solid line through the data points represent a fit by the expression $\frac{C_P}{T} = \gamma + \beta T^2$, where the first term is the normal state electronic contribution and latter one comes from the lattice specific heat. The fit gave the Sommerfeld coefficient γ = 29.4(2) mJ mol^{-1} K^{-2} and β = 0.42(2) mJ mol^{-1} K^{-4}. The Debye temperature is then calculated using the relation: $\Theta_D = \sqrt[3]{\frac{12\pi^4 nR}{5\beta_3}}$, where n is a number of atoms per formula unit (here n = 9) and R is the gas constant (R = 8.31 J mol^{-1} K^{-1}). The obtained value of the Debye temperature is Θ_D = 347(6) K. The resulting value is about 20% lower than the Debye temperature of Aluminum (Θ_D = 428 K [23]) and about 23% higher than the Debye temperature of Zirconium (Θ_D = 290 K [24]). Using previously obtained $\Delta C/T_c$ = 42.8 mJ mol^{-1} K^{-2} and γ = 29.4(2) mJ mol^{-1} K^{-2}, we got $\Delta C/\gamma T_c$= 1.41. This value is very close to the weak coupling superconductivity limit predicted by the BCS theory ($\Delta C/\gamma T_c$=1.43).

Knowing the Debye temperature and T_c, and taking the Coulomb pseudopotential parameter $\mu^\star$ = 0.13 [25–27], the electron – phonon coupling can be estimated from the inverted McMillan

formula [28]: $\lambda_{el-ph} = \frac{1.04+\mu^* \ln\left(\frac{\Theta_D}{1.45T_c}\right)}{(1-0.62\mu^*)\ln\left(\frac{\Theta_D}{1.45T_c}\right)-1.04}$. The value obtained from the calculation is equal to $\lambda_{el\text{-}ph}$ = 0.48, suggesting that Zr_5Al_4 is a weak electron-phonon coupling superconductor. From the Sommerfeld coefficient and the electron-phonon coupling parameter the non-interacting density of states at the Fermi level DOS(E_F) can be estimated via relation: $DOS(E_F) = \frac{3\gamma}{\pi^2 k_B^2(1+\lambda_{el-ph})}$, where k_B is the Boltzmann constant. The calculated $DOS(E_F)$ = 8.4 states per eV per formula unit (f.u.).

Fig. 4b) shows specific heat jump in vicinity of superconducting transition temperature in different applied magnetic fields (0, 0.25 and 0.5 T). Vertical solid lines represent the midpoints of the transitions for each field and will be used for calculation of the upper critical field (Fig. 5(b)). The size of superconducting anomaly becomes smaller and shifts towards lower temperature with increasing magnetic field.

Temperature dependence of electrical resistivity ρ(T) of Zr_5Al_4 is presented in a main panel of Fig. 5. Metallic behavior (dρ(T)/dT > 0) is manifested in the whole temperature range. Below 10 K resistivity becomes temperature independent with a residual resistivity $\rho_r \sim 37$ μΩ cm. The residual resistivity ratio is rather low RRR = $\rho_{300}/\rho_r \approx 2$, which is common for polycrystalline samples [7,29,30]. The data above the superconducting transition was fitted with a parallel resistor model [31–33] in which Bloch-Grüneisen resistivity ρ_{BG} is combined with parallel independent resistor ρ_{max}, as seen on the diagram in Fig. 5. In this model resistivity is described as:

$$\rho(T)^{-1} = \rho_P^{-1} + (\rho_0 + \rho_{BG})^{-1},$$

where

$$\rho_{BG} = 4R\Theta\left(\frac{T}{\Theta}\right)^5 \int \frac{x^5}{(\exp(x)-1)(1-\exp(-x))}dx.$$

The temperature independent resistivity ρ_0 estimated from the fit is 53 μΩ cm, saturation resistivity ρ_{max} = 127 μΩ cm and the characteristic temperature Θ = 202(1) K.

The results of resistivity ρ(T) measurements at low temperatures are shown in Fig. 5(b) to highlight the superconducting transition. The resistivity in zero-field drops below 2.1 K and reaches zero at 1.9 K. The transition temperature T_c = 2.04 K, determined as a midpoint of the resistivity drop, is higher than obtained from heat capacity and magnetic susceptibility measurements. This effect is likely caused by the surface superconductivity phenomena

reported also in the Al containing samples [29,34]. Superconducting transition shifts to lower temperature with increasing magnetic field. These data (red circles), together with the data obtained from the specific heat measurement (blue squares), are shown in Fig. 5(b).

The upper critical field of single-band type-II BCS superconductor can be calculated using the Werthamer-Helfand-Hohenberg (WHH) expression [35,36]:

$$\mu_0 H_{c2}(0) = -AT_C \frac{d\mu_0 H_{c2}}{dT}\Big| T = T_C,$$

where A is the purity factor (0.693 for dirty and 0.73 for clean limit). The slope $\mu_0 \frac{dH_{c2}}{dT} = -0.87 \frac{T}{K}$ is almost identical for both - heat capacity and resistivity series. Taking T_c = 1.82 K we obtained the upper critical field $\mu_0 H_{c2}(0)$ = 1.09 T for dirty and $\mu_0 H_{c2}(0)$ = 1.16 T for clean limit. For a type-II superconductor the superconducting coherence length can be estimated by using the Ginzburg-Landau formula [37] $H_{c2} = \Phi_0/2\pi\xi^2_{GL}$, where Φ_0 = h/2e is the flux quantum. Taking $\mu_0 H_{c2}(0)$ = 1.09 T, the coherence length for Zr_5Al_4 is $\xi_{GL}(0)$ = 173 nm.

The normal and superconducting parameters are listed in Table 2 and compared with the parameters reported for $VAl_{10.1}$ [29,38], ScV_2Al_{20} [7] and $ReGa_5$ [1].

To gain an intrinsic insight into superconductivity and the electronic states of Zr_5Al_4, the electronic density of states (DOS) and band structure of Zr_5Al_4 were investigated with and without spin-orbit coupling (SOC). Fig. 6 a) illustrates the total density of states (DOS) for Zr_5Al_4 with and without SOC. The DOS in the energy below −2.0 eV is contributed mainly from Zr and Al *s* and *d*-orbital. The DOS in the energy range from −2.0 eV to +2.0 eV is primarily mixed by Zr and Al *s*, *d*-, and *p*- orbital, in particular around Fermi level. A sharp peak in the DOS in Zr_5Al_4 is often taken as an indication of a nearby structural, electronic, or magnetic instability such as superconductivity. To unravel it, we calculated the band structure without and with spin-orbit coupling of Zr_5Al_4, presented in Fig. 6 b) and c), respectively. The band structure shows that the peak at the Fermi level in DOS is due to the presence of saddle points in the electronic structure at the M and L points in the Brillouin zone. These saddle points near E_F are often proposed to be important for yielding superconductivity in a variety of materials [39].

The DOS(E_F) from DFT calculations has a value of ~ 15 states per eV per formula unit, which is almost two times higher than value calculated from the Sommerfeld coefficient and the

electron-phonon coupling parameter (8.4 states per eV per formula unit). Using value obtained from the electronic structure calculations, we can estimate the value of electronic heat capacity coefficient $\gamma_{calc}=\frac{\pi^2}{3}k_B^2N(E_F)=35.5$ mJ mol^{-1} K^{-2}, that is again higher than experimental value: $\gamma_{exp}=29.4$ mJ mol^{-1} K^{-2}.

IV Conclusions

We have successfully synthesized a polycrystalline sample of a high-temperature Zr_5Al_4 phase. Powder x-ray diffraction confirms the phase purity and the hexagonal structure in space group $P6_3/mcm$ and lattice parameters a = 8.4312(6) Å and c = 5.7752(8) Å. From magnetic susceptibility, heat capacity and resistivity measurements the material was found to be a type-II superconductor with the transition temperature T_c = 1.82 K. Analysis of the heat capacity data allowed us to estimate the electron-phonon coupling parameter λ_{el-ph} = 0.48, classifying Zr_5Al_4 as a weakly correlated superconductor.

In Table 2 we compare superconducting parameters for Zr_5Al_4 with Al-based ($Val_{10.1}$ and ScV_2Al_{20}) and Ga-based ($ReGa_5$) endohedral superconductors, that have similar critical temperature. All the compounds are weakly coupling superconductors with $\lambda_{el-ph} \sim 0.5$. Different Debye temperature reflects different concentration of the light Al atoms ($Val_{10.1}$ and ScV_2Al_{20}) or presence of a heavier Ga atom in $ReGa_5$. Interestingly, the Sommerfeld coefficient (calculated per mol-at.) is the largest for Zr_5Al_4 and is also reflected by the van Hove singularity scenario as seen in our band structure calculations.

Acknowledgements

The research performed at the Gdansk University of Technology was supported by the National Science Centre (Poland) grant (UMO-2016/22/M/ST5/00435). The work at LSU is supported by Beckman Young Investigator Award.

References

[1] W. Xie, H. Luo, B.F. Phelan, T. Klimczuk, F.A. Cevallos, R.J. Cava, Endohedral gallide cluster superconductors and superconductivity in ReGa5, Proc. Natl. Acad. Sci. 112 (2015) E7048–E7054. doi:10.1073/pnas.1522191112.

[2] P. Neha, P. Sivaprakash, K. Ishigaki, G. Kalaiselvan, K. Manikandan, R.S. Dhaka, Y. Uwatoko, S. Arumugam, S. Patnaik, Nuanced superconductivity in endohedral gallide Mo 8 Ga 41, Mater. Res. Express. 6 (2019) 016002. doi:10.1088/2053-1591/aae5b5.

[3] P. Neha, B. Sharma, S. Patnaik, Synthesis and characterization of binary intermetallic superconductor Mo8Ga41, AIP Conf. Proc. 1832 (2017) 130048. doi:10.1063/1.4980768.

[4] V.Y. Verchenko, R. Khasanov, Z. Guguchia, A.A. Tsirlin, A.V. Shevelkov, Two-gap superconductivity in ${\mathrm{Mo}}_{8}{\mathrm{Ga}}_{41}$ and its evolution upon vanadium substitution, Phys. Rev. B. 96 (2017) 134504. doi:10.1103/PhysRevB.96.134504.

[5] J. Zhou, S. Zhang, Q. Wang, P. Jena, Integrating superconducting phase and topological crystalline quantum spin Hall effect in hafnium intercalated gallium film, Appl. Phys. Lett. 108 (2016) 253102. doi:10.1063/1.4954672.

[6] W. Xie, E.M. Seibel, R.J. Cava, The New Superconductor tP-SrPd2Bi2: Structural Polymorphism and Superconductivity in Intermetallics, Inorg. Chem. 55 (2016) 3203–3205. doi:10.1021/acs.inorgchem.5b02900.

[7] M.J. Winiarski, B. Wiendlocha, M. Sternik, P. Wiśniewski, J.R. O'Brien, D. Kaczorowski, T. Klimczuk, Rattling-enhanced superconductivity in $M{\mathrm{V}}_{2}\mathrm{A}{\mathrm{l}}_{20}\phantom{\rule{0.28em}{0ex}}(M=\mathrm{Sc},\phantom{\rule{0.16em}{0ex}}\mathrm{Lu},\phantom{\rule{0.16em}{0ex}}\mathrm{Y})$ intermetallic cage compounds, Phys. Rev. B. 93 (2016) 134507. doi:10.1103/PhysRevB.93.134507.

[8] M. Tsujimoto, Y. Matsumoto, T. Tomita, A. Sakai, S. Nakatsuji, Heavy-Fermion Superconductivity in the Quadrupole Ordered State of ${\mathrm{PrV}}_{2}{\mathrm{Al}}_{20}$, Phys. Rev. Lett. 113 (2014) 267001. doi:10.1103/PhysRevLett.113.267001.

[9] K. Matsubayashi, T. Tanaka, A. Sakai, S. Nakatsuji, Y. Kubo, Y. Uwatoko, Pressure-Induced Heavy Fermion Superconductivity in the Nonmagnetic Quadrupolar System ${\mathrm{PrTi}}_{2}{\mathrm{Al}}_{20}$, Phys. Rev. Lett. 109 (2012) 187004. doi:10.1103/PhysRevLett.109.187004.

[10] A. Yamada, R. Higashinaka, T.D. Matsuda, Y. Aoki, Superconductivity in Cage Compounds LaTr2Al20 with Tr = Ti, V, Nb, and Ta, J. Phys. Soc. Jpn. 87 (2018) 033707. doi:10.7566/JPSJ.87.033707.

[11] E.J. Little, M.M. Jones, A complete table of electronegativities, J. Chem. Educ. 37 (1960) 231. doi:10.1021/ed037p231.

[12] R.V. Nandedkar, P. Delavignette, On the Formation of a New Superstructure in the Zirconium-Aluminium System, Phys. Status Solidi A. 73 (1982) K157–K160. doi:10.1002/pssa.2210730246.

[13] T.J. Renouf, C.A. Beevers, The crystal structure of Zr2Al3, Acta Crystallogr. 14 (1961) 469–472. doi:10.1107/S0365110X61001510.

[14] T.J. Renouf, A comparison of the structures Zr2Al3 and ZrAl2, Acta Crystallogr. 15 (1962) 282–283. doi:10.1107/S0365110X6200064X.

[15] M. Alatalo, M. Weinert, R.E. Watson, Stability of Zr-Al alloys, Phys. Rev. B. 57 (1998) R2009–R2012. doi:10.1103/PhysRevB.57.R2009.

[16] K. Persson, Materials Data on Zr5Al4 (SG:193) by Materials Project, (2016). doi:10.17188/1275900.

[17] G.S. Pawley, Unit-cell refinement from powder diffraction scans, J. Appl. Crystallogr. 14 (1981) 357–361. doi:10.1107/S0021889881009618.
[18] A.A. Coelho, TOPAS Academic: General Profile and Structure Analysis Software for Powder Diffraction Data, Bruker AXS, Karlsruhe, Germany, 2007.
[19] A. Jain, S.P. Ong, G. Hautier, W. Chen, W.D. Richards, S. Dacek, S. Cholia, D. Gunter, D. Skinner, G. Ceder, K. a. Persson, The Materials Project: A materials genome approach to accelerating materials innovation, APL Mater. 1 (2013) 011002. doi:10.1063/1.4812323.
[20] K. Persson, Materials Data on Zr4Al3 (SG:191) by Materials Project, (2014). doi:10.17188/1189164.
[21] K. Persson, Materials Data on Zr2Al3 (SG:43) by Materials Project, (2015). doi:10.17188/1190927.
[22] T. Klimczuk, R.J. Cava, Carbon isotope effect in superconducting $\mathrm{Mg}\mathrm{C}{\mathrm{Ni}}_{3}$, Phys. Rev. B. 70 (2004) 212514. doi:10.1103/PhysRevB.70.212514.
[23] Charles Kittel-8th Edition, Introduction to Solid State Physics, n.d. http://archive.org/details/IntroductionToSolidStatePhysics (accessed December 14, 2016).
[24] A. Tari, The specific heat of matter at low temperatures., Imperial College Press, London, 2003.
[25] L.C. Srivichitranond, E.M. Seibel, W. Xie, Z. Sobczak, T. Klimczuk, R.J. Cava, Superconductivity in a new intermetallic structure type based on endohedral $\mathrm{Ta}@\mathrm{I}{\mathrm{r}}_{7}\mathrm{G}{\mathrm{e}}_{4}$ clusters, Phys. Rev. B. 95 (2017) 174521. doi:10.1103/PhysRevB.95.174521.
[26] V.Y. Verchenko, A.A. Tsirlin, A.O. Zubtsovskiy, A.V. Shevelkov, Strong electron-phonon coupling in the intermetallic superconductor ${\mathrm{Mo}}_{8}{\mathrm{Ga}}_{41}$, Phys. Rev. B. 93 (2016) 064501. doi:10.1103/PhysRevB.93.064501.
[27] D. Singh, A.D. Hillier, A. Thamizhavel, R.P. Singh, Superconducting properties of the noncentrosymmetric superconductor ${\mathrm{Re}}_{6}\mathrm{Hf}$, Phys. Rev. B. 94 (2016) 054515. doi:10.1103/PhysRevB.94.054515.
[28] W.L. McMillan, Transition Temperature of Strong-Coupled Superconductors, Phys. Rev. 167 (1968) 331–344. doi:10.1103/PhysRev.167.331.
[29] T. Klimczuk, M. Szlawska, D. Kaczorowski, J.R. O'Brien, D.J. Safarik, Superconductivity in the Einstein solid V Al 10.1, J. Phys. Condens. Matter. 24 (2012) 365701. doi:10.1088/0953-8984/24/36/365701.
[30] T. Klimczuk, C.H. Wang, K. Gofryk, F. Ronning, J. Winterlik, G.H. Fecher, J.-C. Griveau, E. Colineau, C. Felser, J.D. Thompson, D.J. Safarik, R.J. Cava, Superconductivity in the Heusler family of intermetallics, Phys. Rev. B. 85 (2012) 174505. doi:10.1103/PhysRevB.85.174505.
[31] H. Wiesmann, M. Gurvitch, H. Lutz, A. Ghosh, B. Schwarz, M. Strongin, P.B. Allen, J.W. Halley, Simple Model for Characterizing the Electrical Resistivity in $A\ensuremath{-}15$ Superconductors, Phys. Rev. Lett. 38 (1977) 782–785. doi:10.1103/PhysRevLett.38.782.
[32] C.H. Wang, J.M. Lawrence, E.D. Bauer, K. Kothapalli, J.S. Gardner, F. Ronning, K. Gofryk, J.D. Thompson, H. Nakotte, F. Trouw, Unusual signatures of the ferromagnetic transition in the heavy fermion compound ${\text{UMn}}_{2}{\text{Al}}_{20}$, Phys. Rev. B. 82 (2010) 094406. doi:10.1103/PhysRevB.82.094406.
[33] T. Klimczuk, C.H. Wang, J.M. Lawrence, Q. Xu, T. Durakiewicz, F. Ronning, A. Llobet, F. Trouw, N. Kurita, Y. Tokiwa, H. Lee, C.H. Booth, J.S. Gardner, E.D. Bauer, J.J. Joyce, H.W. Zandbergen, R. Movshovich, R.J. Cava, J.D. Thompson, Crystal fields,

disorder, and antiferromagnetic short-range order in Yb${}_{0.24}$Sn${}_{0.76}$Ru, Phys. Rev. B. 84 (2011) 075152. doi:10.1103/PhysRevB.84.075152.
[34] R.W. Cohen, B. Abeles, Superconductivity in Granular Aluminum Films, Phys. Rev. 168 (1968) 444–450. doi:10.1103/PhysRev.168.444.
[35] N.R. Werthamer, E. Helfand, P.C. Hohenberg, Temperature and Purity Dependence of the Superconducting Critical Field, ${H}_{c2}$. III. Electron Spin and Spin-Orbit Effects, Phys. Rev. 147 (1966) 295–302. doi:10.1103/PhysRev.147.295.
[36] E. Helfand, N.R. Werthamer, Temperature and Purity Dependence of the Superconducting Critical Field, ${H}_{c2}$. II, Phys. Rev. 147 (1966) 288–294. doi:10.1103/PhysRev.147.288.
[37] M. Tinkham, Introduction to Superconductivity, Courier Corporation, 1996.
[38] D.J. Safarik, T. Klimczuk, A. Llobet, D.D. Byler, J.C. Lashley, J.R. O'Brien, N.R. Dilley, Localized anharmonic rattling of Al atoms in VAl${}_{10.1}$, Phys. Rev. B. 85 (2012) 014103. doi:10.1103/PhysRevB.85.014103.
[39] W. Xie, H. Luo, E.M. Seibel, M.B. Nielsen, R.J. Cava, Superconductivity in Hf5Sb3–xRux: Are Ru and Sb a Critical Charge-Transfer Pair for Superconductivity?, Chem. Mater. 27 (2015) 4511–4514. doi:10.1021/acs.chemmater.5b01655.
[40] K. Momma, F. Izumi, VESTA 3 for three-dimensional visualization of crystal, volumetric and morphology data, J. Appl. Crystallogr. 44 (2011) 1272–1276. doi:10.1107/S0021889811038970.

Figure 1

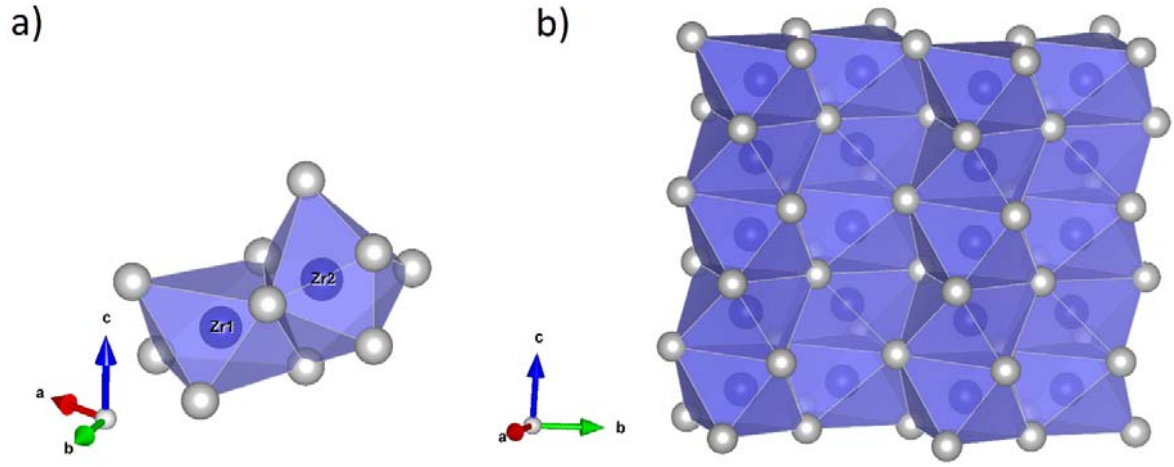

Fig. 1 Crystal structure of Zr_5Al_4.Zirconium and aluminum atoms are represented by blue and silver balls, respectively.1 a) Trigonal bipyramidal cluster of Al around Zr1 atom and double decahedral cluster of Al surrounding Zr2 atom b) Set of double decahedral clusters of Al atoms surrounding Zr1 atoms in unit cell. Image rendered using VESTA [40].

Figure 2

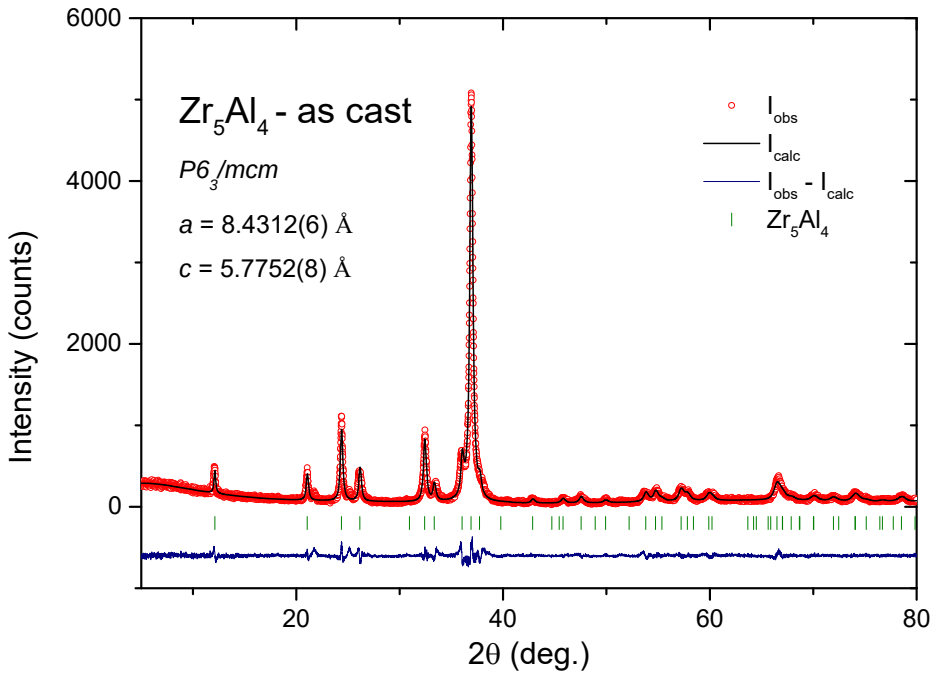

Fig. 2 The X-ray powder diffraction characterization of a crushed Zr_5Al_4 as-cast sample. The plot shows the Pawley fit (black solid line) to the measured intensity (red dots). The blue line shows the difference between measured and calculated intensity. Green ticks represent the expected positions of Bragg reflections for Zr_5Al_4 compound.

Figure 3

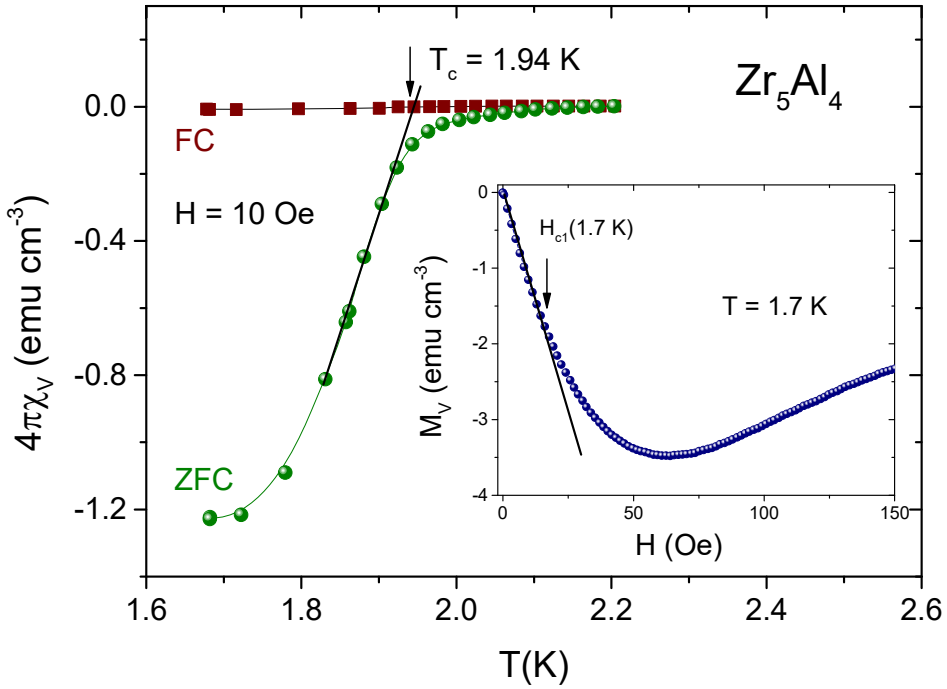

Fig. 3 Main Panel: The zero-field cooled (ZFC) and field cooled (FC) volume susceptibility $\chi_V(T)$ through the superconducting transition, measured in a field of 10 Oe. Inset: magnetization vs. magnetic field M(H) at T=1.7 K.

Figure 4

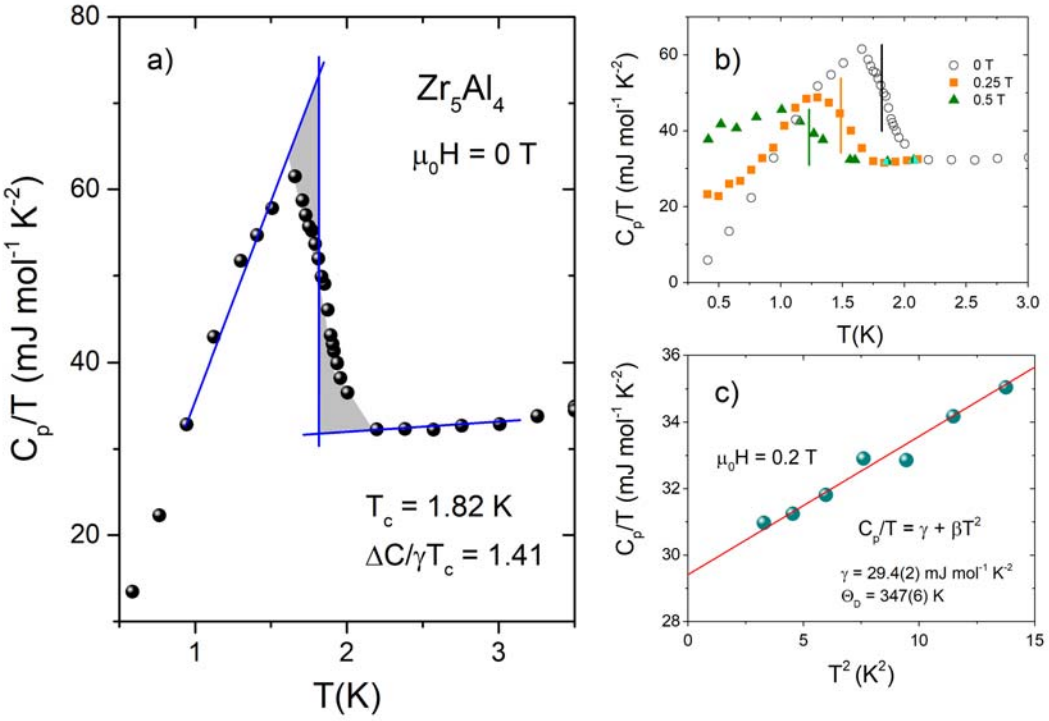

Fig. 4. Low temperature specific heat of Zr_5Al_4. (a) Superconducting anomaly under zero applied magnetic field. The size of the anomaly is estimated using the conserved entropy construction, (b) superconducting transition in different applied magnetic fields, (c) C_p/T vs, T^2 in the normal state region, measured in magnetic field of 0.2 T

Figure 5

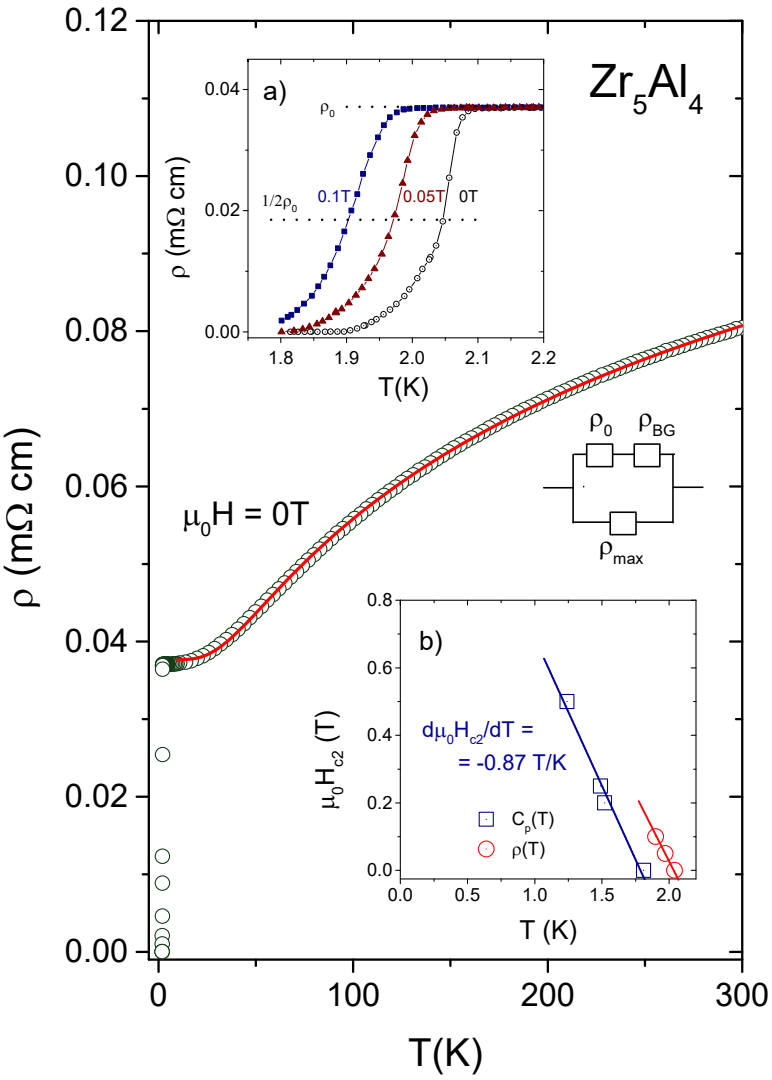

Fig. 5. Electrical resistivity of Zr_5Al_4. Main Panel: resistivity over a wide temperature range fitted with parallel resistor model, (a) Resistivity data near the superconducting transition in fields from 0 to 0.1 T, (b) Upper critical field as a function of temperature plotted with data from heat capacity (squares) and resistivity (circles) measurements.

Figure 6

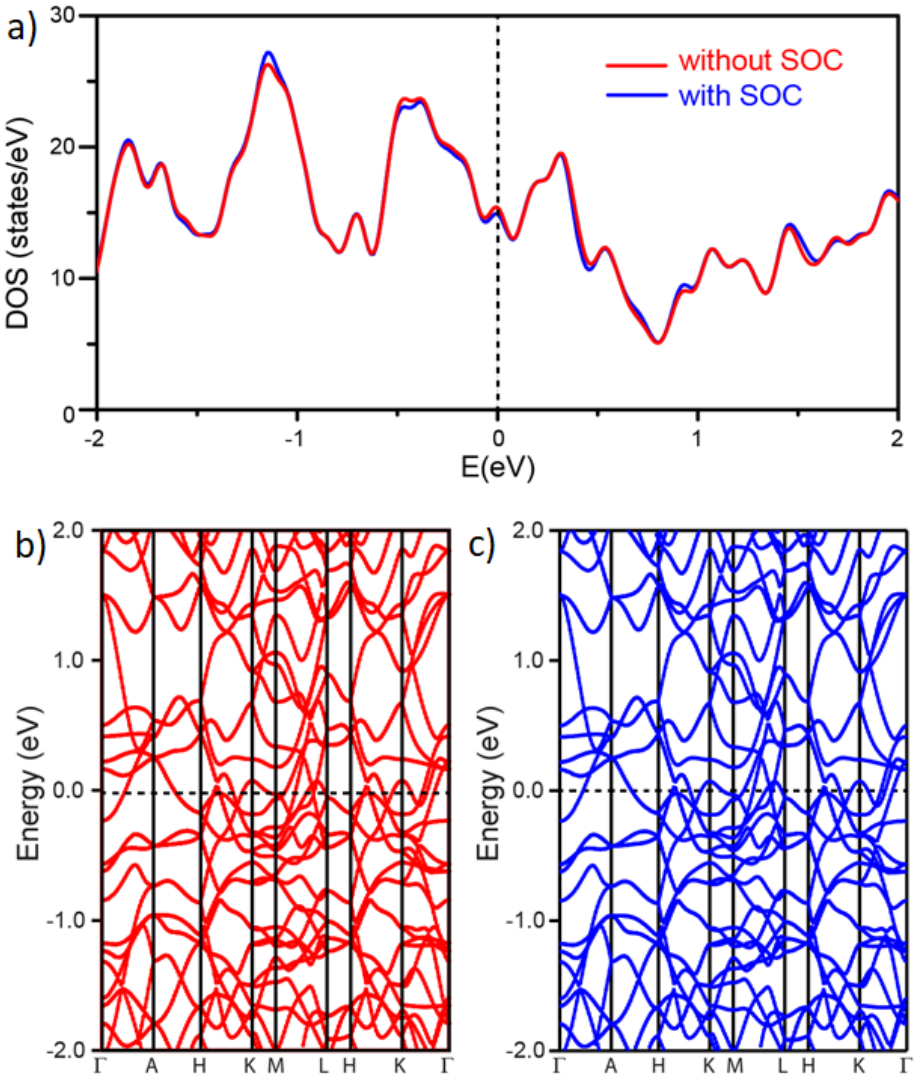

Fig. 5. (a) The total density of states (DOS) for Zr_5Al_4 with and without SOC. Bottom: The band structure (b) without and (c) with spin-orbit coupling for Zr_5Al_4

Table 1

Table 1 Crystallographic data for Zr_5Al_4. Cell parameters obtained from the Pawley fit are compared with the values reported by Nandedkar and Delavignette [12]. Figures of merit are R_p(%) = 8.72, R_{wp}(%) = 11.81, R_{exp}(%) = 8.57, χ^2 = 1.38.

Zr_5Al_4		
Space group	*P6₃/mcm* (# 193)	
Pearson symbol	hP18	
Cell parameters (Å)	Pawley fit:	Ref.[12]:
a =	8.4312(6)	8.447
c =	5.7752(8)	5.81
Cell volume (Å^3)	355.53(7)	359.01
Molar weight (g/mol)	564.05	
Number of formula units per cell – *Z*	2	
Density (calculated) (g/cm^3)	5.27	5.22

Table 2

Table 2 Values of the normal and superconducting parameters of Zr_5Al_4 compared with ScV_2Al_{20} [7], $VAl_{10.1}$ [29,38] and $ReGa_5$ [1]. The T_c for Zr_5Al_4 was estimated from the specific heat measurement.

parameter	**Zr_5Al_4 [this work]**	**ScV_2Al_{20} [7]**	**$VAl_{10.1}$ [29,38]**	**$ReGa_5$ [1]**
T_c (K)	1.82	1.00	1.53	2.1
γ (mJ mol^{-1} K^{-2}) (mJ mol-at.$^{-1}$ K^{-2})	 29.4(2) 3.3	 29.6 1.3	 17.3 1.56	 4.7 0.8
Θ_D (K)	367	536	341	314
$\Delta C_{el}/\gamma T_c$	1.41	1.46	1.42	1.6
$\lambda_{el\text{-}ph}$	0.48	0.41	0.42 / 0.51	0.51
$DOS(E_F)$ (eV^{-1} per f.u.)	8.4	9.00	5.2 / 4.9	1.3
$H_{c2}(0)$ (T)	1.09 (dirty limit) 1.15 (clean limit)	0.333(4)	0.1	---
ξ_{GL} (Å)	173	314	800	-